



Cite this: DOI: 10.1039/c5ta03210e

Charge transfer processes at the semiconductor/ electrolyte interface for solar fuel production: insight from impedance spectroscopy†

Luca Bertoluzzi,^{*a} Pilar Lopez-Varo,^b Juan Antonio Jiménez Tejada^b
and Juan Bisquert^{ac}

Knowledge of the nature of charge transfer processes at the semiconductor/electrolyte interface is crucial for the optimization of semiconductors used for solar fuel production. In the literature, there are two types of charge transfer mechanisms: (i) direct hole transfer from the valence band and (ii) indirect hole transfer *via* surface states. In this paper, we discuss both processes in the steady state regime through full drift-diffusion simulations considering the concomitant influence of the electric field and surface states at the semiconductor/electrolyte interface. We discuss the role of surface states and valence band holes in the photo-anodic current. We subsequently analyze both hole transfer processes in a dynamic regime *via* the impedance spectroscopy (IS) method. We provide a solid criterion to discriminate both mechanisms and discuss some experimental examples from the literature.

Received 1st May 2015
Accepted 24th June 2015

DOI: 10.1039/c5ta03210e

www.rsc.org/MaterialsA

Introduction

The current quest for efficient, clean and cheap energy sources has led to active investigation for alternatives to classical energy production and storage methods. One promising solution is solar fuel production, which allows transforming solar energy into chemical energy by electrochemical processes with the use of light absorbing semiconductors and catalysts.^{1,2}

However, semiconductors used for solar fuel production must fulfill several conditions which include the low cost of the materials, their earth abundance, absorption in the visible region and long term stability in solution.^{3,4} The sum of all these conditions results in an overall stringent selection criterion, which reduces the panel of available semiconductors to only a few materials. A few set of wide bandgap metal oxides TiO₂,⁵ BiVO₄,⁶ WO₃,⁷ and Fe₂O₃,^{8,9} which are n-type materials, are favored because of their stability and suitable energetics for use as photoanodes for the water oxidation reaction.

Even though these materials are promising, they still display sluggish oxidation kinetics.¹⁰ Two causes have been identified in the literature: (i) slow transfer of holes toward the solution and (ii) fast electron hole recombination. The first possibility

can be justified by the necessity to transfer four holes for water oxidation.¹¹ The second one can be justified by the presence of a significant density of inner band gap surface states, which is a feature of many oxide semiconductors. Nonetheless, these states may not only act as recombination centers but may also play an important role in the hole transfer process, depending on the physicochemical nature of the semiconductor/electrolyte interface.¹²

In recent years, it has been broadly recognized that the functions of light absorption, charge separation and charge transfer can be decoupled forming devices that combine a photoactive layer with suitable catalysts and protection layers.^{13,14} Furthermore, the high voltage needed for the water splitting reaction in combination with the requirement of high photon collection efficiency recommends the coupling of several middle size bandgap semiconductors to form efficient tandem devices.¹⁵ Even though a light absorbing semiconductor is supplemented with several layers, the operation of such layers in terms of recombination and charge transfer processes still needs to be understood.

In general, for the characterization of the photoinduced oxygen evolution reaction (OER), it is necessary to distinguish two competing types of charge transfer processes at the semiconductor/electrolyte interface, which are shown in Fig. 1. The first one is direct hole transfer from the valence band while the second one, which we have recently discussed,¹⁶ is indirect charge transfer from surface states at low bias and from the valence band at higher bias. This latter process may also represent an intermediate reaction step where photo-generated holes are captured in surface adsorbed species.¹⁷ It should be also pointed out that both types of processes, direct and indirect, may

^aInstitute of Advanced Materials (INAM), Universitat Jaume I, 12071 Castelló, Spain.
E-mail: bertoluz@uji.es

^bDepartamento de Electrónica y Tecnología de Computadores, CITIC-UGR, Universidad de Granada, 18071 Granada, Spain

^cDepartment of Chemistry, Faculty of Science, King Abdulaziz University, Jeddah, Saudi Arabia

† Electronic supplementary information (ESI) available. See DOI: 10.1039/c5ta03210e

occur at the same time in parallel pathways. This is the case, for example, of the semiconductor surface that supports a porous catalyst, when both are in direct contact with the electrolyte.

In order to discriminate between direct and indirect transfer mechanisms, several studies have been performed in the dynamic regime.^{10,18,19} One approach consists of measuring the hole chemical capacitance, which can be achieved by impedance spectroscopy (IS).²⁰ Such capacitance reflects the variation in carrier concentration in a given storage mode (in this case,

either surface states or valence band) when the system undergoes a change in the Fermi level. In this paper, we show calculations of steady state current through full drift-diffusion simulations and the corresponding IS behavior in the dynamic regime and we discuss the two main hole transfer processes proposed in the literature. We provide the main criterion which allows differentiating direct and indirect charge transfer through low frequency capacitance measurements.

Model

Let us first discuss the general framework depicted in Fig. 1a, which underlies the model of Fig. 1b, where only direct charge transfer from the valence band is considered, and the one of Fig. 1c, where concomitant indirect charge transfer from surface states and direct charge transfer from the valence band are taken into account. We consider here an n-type semiconductor of length L with a rectifying selective contact for holes at the semiconductor/electrolyte interface and an ohmic selective contact for electrons at the metal/semiconductor one. In this configuration, the applied voltage, V , regulates the height of the Schottky barrier seen from the semiconductor at the semiconductor/electrolyte interface. The concentration of electrons at the ohmic electron selective contact is constant and equal to the equilibrium concentration, n_0 . At the interface, whose spatial extension is δL , holes can either oxidize water or recombine. The oxidation reaction is facilitated in reverse bias when the electric field in the depletion region is increased and holes accumulate in this region.

We have developed simulations of this model system solving numerically the full set of drift-diffusion equations under illumination detailed in the ESI.† \bar{n} electrons and \bar{p} holes per unit volume are photo-generated at a rate $G = \alpha\phi_0 \exp(-\alpha x)$, where α is the absorption coefficient and ϕ_0 is the photon flux. They can recombine at a rate $U_r = B(\bar{n}\bar{p} - n_0p_0)$, B being the recombination constant and p_0 being the equilibrium concentration of holes. In particular, the assumption of the constant Fermi level of the majority carrier shown in Fig. 1a is not adopted, as the model includes a position dependent recombination rate. In Fig. 2 we present the results of current voltage characteristics and the corresponding hole density at the semiconductor/electrolyte interface as a function of the applied voltage for both models of Fig. 1b and c. In Fig. 2a, a first plateau is observed at low bias, which corresponds to strong electron-hole recombination and a very small current. When the onset voltage is reached, the barrier height is high and the electric field increases, favoring charge separation and reducing recombination. This is when the anodic current increases. Note that this onset voltage strongly depends on the charge transfer process involved in the oxidation reaction. We will discuss this point later on. When the electric field is large enough, recombination is completely suppressed, all the photo-generated holes are collected at the interface, and the concentration of holes at the semiconductor/electrolyte interface is constant, as shown in Fig. 2b, independent of the nature of the charge transfer process. For this reason, the current reaches a plateau at higher anodic bias.

Let us now analyze in more detail the influence of the charge transfer process on the current-voltage characteristics. For

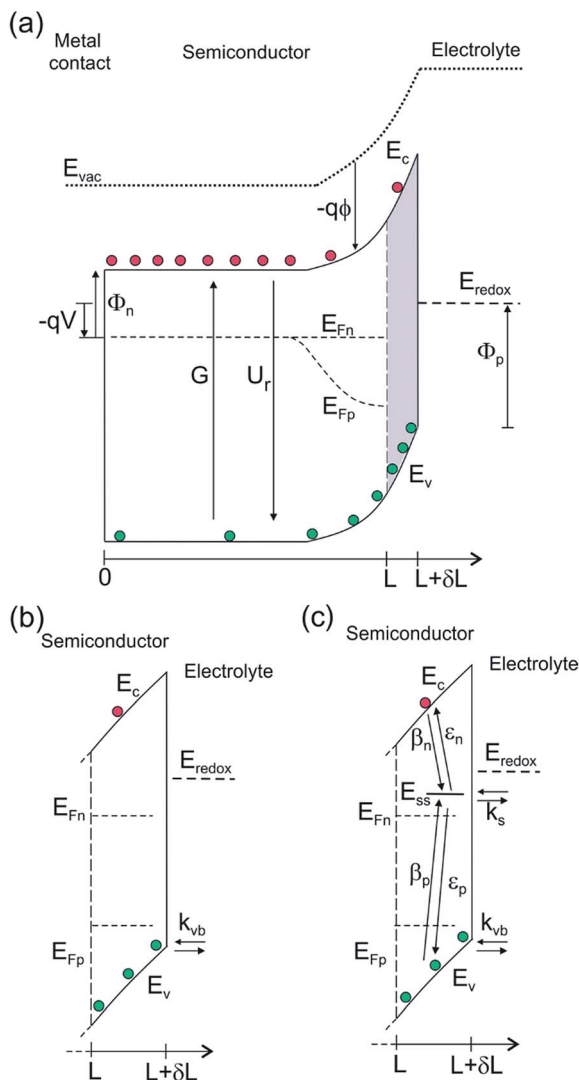


Fig. 1 (a) Energy diagrams of an n-type semiconductor of thickness L where electrons and holes are generated at a rate G and recombine at a rate U_r . At the interface of length δL , hole transfer to the redox level E_{redox} can take place (b) directly from the valence band (kinetic constant k_{vb}) and (c) indirectly from surface states at low bias and directly from the valence band at higher bias. In this latter model, we consider trapping of electrons and holes (β_n and β_p) and detrapping (ϵ_n , ϵ_p) and hole transfer from surface states (k_s) at the energy level E_{ss} , in competition with direct hole transfer. In these schemes E_c and E_v are the energies of the lower edge of the conduction band and the higher edge of the valence band, respectively. E_{Fn} and E_{Fp} are the quasi Fermi levels, Φ_n and Φ_p are the injection barriers of electrons and holes, E_{vac} is the local vacuum level, ϕ is the local electrostatic potential and V is the applied voltage.

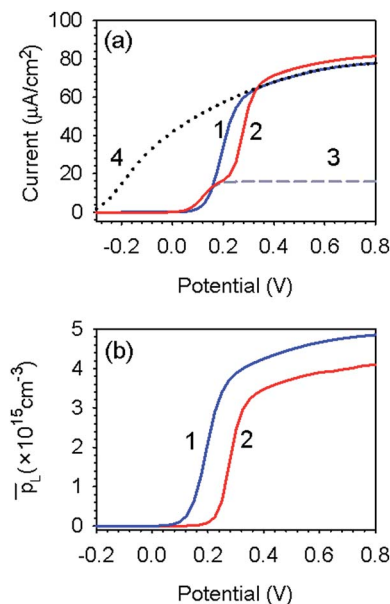


Fig. 2 (a) Full drift diffusion simulations of the current voltage plots when holes are directly transferred from the valence band, as depicted by the model in Fig. 1b (1) and when direct hole transfer competes with indirect charge transfer from the surface states, as shown by the model in Fig. 1c (2). The current associated with hole transfer from the traps, in the framework of this latter model, is represented in grey dashed lines (3). We also indicate the J - V curve for a perfect hole selective contact without surface states (4). (b) Corresponding hole density in the valence band at the semiconductor/electrolyte interface ($x = L$) as a function of the applied voltage. The parameters used for these simulations are summarized in Table S1.†

more clarity we consider all the charge transfer kinetic constants as being independent of the distribution of the donor states in the electrolyte. A more detailed analysis of charge transfer processes in the framework of the Marcus model can be found elsewhere.²¹ For direct charge transfer (plot 1 in Fig. 2), the photo-generated holes are directly extracted from the valence band (at a constant rate k_{vb}) and the photocurrent follows the voltage variations of the hole density at the surface. Note that in this case the maximum achievable photo-anodic current can be approximated within the framework of the Reichman model.²² This approach has been extensively discussed in the literature and for a detailed review of this model we refer the reader to ref. 23.

For indirect charge transfer (plot 2 in Fig. 2), the photo-generated holes are trapped in surface states (hole trapping, β_p , and detrapping, ϵ_p), at the level E_{ss} with a density of surface states per unit volume N_{ss} . The trapped holes can subsequently oxidize water (k_s) or recombine with trapped electrons (electron trapping rate β_n and detrapping rate ϵ_n). In many semiconductors, these states are distributed within the gap of the semiconductor, and most commonly follow exponential and Gaussian distributions. However, the distribution of surface states does not affect the following discussion and, for the sake of concision, we consider here a mono-energetic density of surface states. In this case, the photo-anodic current increases when the surface state assisted recombination decreases, *i.e.*

when the population of trapped electrons decreases. When the surface states are being filled with holes, the anodic current reaches a first plateau corresponding to the maximum achievable current from the surface states. This plateau is indicated by the grey dashed lines in Fig. 2a (plot 3). After reaching the first plateau, the photo-anodic current keeps on increasing, along with the hole density in the valence band, which saturates once the surface state assisted recombination has been totally eliminated by the withdrawal of electrons from the surface.

At this point several remarks should be made on the nature of the anodic current depicted in Fig. 2a (plot 2). First of all, there are two contributions to the total photo-anodic current: the surface state current and the one from the valence band. It must be pointed out that the current from surface states finds its origin in the removal of the electrons present at equilibrium in these states, either by capture of photogenerated holes (β_p) or by detrapping of electrons from these states to the conduction band (ϵ_n) when applying an anodic bias. In other words, the anodic current from these states originates not only from photo-generation but also from the applied bias. For this reason the maximum achievable anodic current can be higher than the photo-generated current with surface states than without surface states, as observed in Fig. 2a. However, the maximum achievable anodic current depends on the recombination kinetics, as suggested by Fig. S1.† Secondly, it should be remarked that the onset voltage depends on the electron detrapping (ϵ_n) and charge transfer (k_s) kinetics.¹⁶ In particular, higher charge transfer kinetics may result in a smaller onset voltage in the presence of surface states. Surface states may therefore be an asset for solar fuel production if the kinetics of indirect charge transfer can be enhanced, as suggested by Fig. 2a. It is therefore crucial to identify the origin of the low bias charge transfer process in order to optimize solar fuel production.

Salvador and coworkers²⁴ have already proposed a criterion in order to discriminate between direct and indirect hole transfer processes under steady state conditions. They demonstrated that the photocurrent depends on illumination as $\alpha\phi_0$ for direct charge transfer and as $\sqrt{\alpha\phi_0}$ for indirect charge transfer. However, this statement holds only under low recombination conditions. For a more general approach, a dynamic study is necessary. A very popular method is IS, which allows decoupling faradic processes (in this case charge transfer and recombination processes) by activating capacitive processes *via* a small frequency dependent perturbation of voltage. IS measurements are usually represented in terms of complex plane plots where the imaginary part of the measured impedance is represented as a function of its real part. In this representation, the resulting patterns are semicircles which can be analyzed with the use of equivalent electrical circuits (ECs). For each semicircle, one capacitance and one resistance values can be extracted. For the case of fuel production with wide band gap semiconductors, a maximum of two semicircles is generally observed, depending on the applied voltage. As a result, two resistance and capacitance values can be obtained from such measurements. The extraction of these latter elements and the adequate physical interpretation of the model rely first of all on the suitable choice of the EC.

In view of the previous considerations, we shall now discuss the ECs presented in Fig. 3 for both hole transfer models. Note that for the sake of clarity, in the following discussion we neglect the transport limitations and all quantities are therefore considered constant. Moreover, since we consider the low bias regime, we can neglect charge transfer from the valence band in the case of Fig. 1c. Under these assumptions, the ECs for the systems presented in Fig. 1b and c are shown in Fig. 3a and b. More details on the calculation of such ECs are given in the ESI.† The EC in Fig. 3a is a simplification of the general transmission line model presented in a recent publication²⁵ with an additional charge transfer resistance for holes from the valence band and without the dielectric relaxation channel. From this EC, we can extract values for two capacitances and resistances, which are associated with the conduction and valence band carriers. The EC in Fig. 3b corresponds to the classical EC for the trapping/detrapping and charge transfer of a single type of carrier.^{26,27} We have already discussed in detail this EC with the additional contribution of valence band holes.¹⁶ In this configuration, we predicted the theoretical possibility of three semi-circles in the complex plane. However, in the present discussion we omit the direct hole transfer from the valence band which takes place at higher voltages and the low frequency arc corresponding to the valence band hole transfer disappears. Then, the circuit in Fig. 3b allows extracting values for two resistances and two capacitances, which are associated with the conduction band and surface states. Note that in this configuration, it is impossible to probe the hole population and consequently extract the recombination resistance associated with electron hole recombination in the surface states. For the latter purpose, other techniques are needed, such as Intensity Modulated Photocurrent Spectroscopy (IMPS),²⁸ where light intensity modulations allow us to directly vary and probe the hole concentration in the valence band.

Interestingly, both ECs presented in Fig. 3 are identical but the physical nature of the electrical elements is different. Of particular interest are the low frequency capacitances, which give valuable information on the storage mode of the photo-generated holes which are involved in the water photo-oxidation. For the EC in Fig. 3a, the low frequency capacitance is associated with valence band holes with concentration \bar{p}_L at the semiconductor/electrolyte interface:

$$C_{\mu}^{(\text{vb})} = \frac{q^2 L}{k_B T} \bar{p}_L \quad (1)$$

For Fig. 3b, the low frequency capacitance is associated with the holes in the surface states and it is written as:

$$C_{\mu\text{p}}^{(\text{ss})} = \frac{q^2 \delta L}{k_B T} B_{\text{ss}}^{-1} \bar{f} (1 - \bar{f}) N_{\text{ss}} \quad (2)$$

where \bar{f} is the steady state electron occupation probability of the surface states at the semiconductor/electrolyte interface ($x = L$) and B_{ss} is a factor such that $0 < B_{\text{ss}} \leq 1$. \bar{f} and B_{ss} are defined by:

$$\bar{f} = \frac{\beta_n \bar{n}_L + k_s f_0 - GL / (N_{\text{ss}} \delta L)}{\beta_n \bar{n}_L + \epsilon_n + k_s} \quad (3)$$

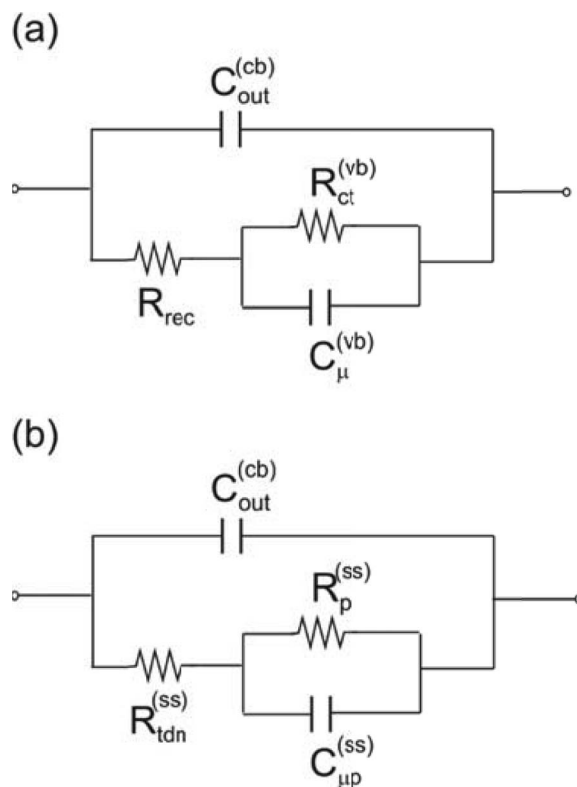


Fig. 3 Equivalent circuit (EC) obtained from a small ac perturbation for (a) the direct hole transfer model in Fig. 1b and (b) the indirect hole transfer model in Fig. 1c. In these circuits, $C_{\text{out}}^{(\text{cb})}$ is the semiconductor capacitance, $C_{\mu}^{(\text{vb})}$ is the valence band equilibrium chemical capacitance, R_{rec} is the band to band recombination resistance, $R_{\text{ct}}^{(\text{vb})}$ is the hole transfer resistance from the valence band, $R_{\text{tdn}}^{(\text{ss})}$ is the trapping/detrapping resistance of electrons from the conduction band and $R_{\text{p}}^{(\text{ss})}$ is the hole transfer resistance from the surface states.

$$B_{\text{ss}} = \left(1 + \frac{\epsilon_n}{\beta_n \bar{n}_L} \right) \bar{f} \quad (4)$$

In eqn (3) and (4), \bar{n}_L is the steady state density of electrons at the interface semiconductor/electrolyte.

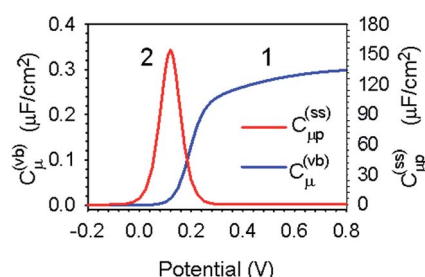


Fig. 4 Low frequency capacitances for the direct charge transfer model in Fig. 1b (1) and the indirect charge transfer model in Fig. 1c (2). The former one is associated with hole storage in the valence band while the latter one is related to hole accumulation in surface states. The steady state electrical magnitudes and parameters involved in the calculations of these capacitances (eqn (1)–(4)) are the ones obtained from the full drift-diffusion simulations shown in Fig. 2.

Both capacitances are represented as a function of voltage in Fig. 4. The voltage dependence for both types of capacitances is clearly different. In fact, the surface state capacitance reaches a peak which marks the transition between occupied (filled with electrons) and unoccupied (filled with holes) surface states. In contrast, the valence band chemical capacitance is directly proportional to the concentration of holes in the valence band and reaches saturation at higher voltages, as suggested by Fig. 2b. Thus, low frequency capacitance measurements are a powerful tool for the distinction between direct and indirect charge transfer.

Discussion

The presence of surface states at the semiconductor/electrolyte interface not only depends on the morphology of the semiconductor surface but also on the nature and composition of the electrolyte. TiO_2 is certainly one of the most popular examples that can be found in the literature.²⁹ In particular, nano-structured TiO_2 shows two types of defects:^{30,31} (i) an exponential tail of defects which arises from the under-coordinated four-fold coordinated surface Ti³² and (ii) a mono-energetic level of Ti interstitials/oxygen vacancies that are due to uncoordinated Ti surface ions.³³ This latter type of defect evolves as OH radicals under illumination in an aqueous electrolyte and can be involved in the photogeneration of H_2O_2 , which in turn adsorbs on the TiO_2 surface and acts as a temporary surface state.^{17,34} Recently, Reckers *et al.* showed that in addition to the deposition method, synchrotron exposure can also strongly influence the density of deep and shallow inner band gap states.³⁵

In the case of $\alpha\text{-Fe}_2\text{O}_3$ (hematite), a clear capacitive peak has been observed, which unveiled charge transfer from the surface states in aqueous solution.¹² These states have the particularity that they can only be observed at anodic bias and under illumination.³⁶ In addition, hematite surface states are strongly dependent on the nature of the electrolyte. A recent study has shown that in the presence of water, methanol or acetonitrile, the distribution of hematite surface states drastically changes.⁹ Moreover, Iandolo and Hellman³⁷ demonstrated an anodic shift of the surface state capacitive peak with pH. These authors analyzed the nature of the surface states involved in the capacitive response with DFT calculations. They showed that the Fe_2O_3 surface is populated with two types of terminations: $-\text{O}$ and $-\text{OH}$, which both act as surface states. $-\text{OH}$ induced states are close to the middle of the semiconductor band gap and act as recombination centers at low bias, while $-\text{O}$ terminations are close to the valence band and allow hole transfer at higher bias. Both states were observed using impedance spectroscopy and cyclic voltammetry by Klahr and Hamann³⁸ for hematite in an aqueous electrolyte. The same group concomitantly showed that the surface states identified as recombination centers could be selectively removed by using atomic layer deposition (ALD) and annealing hematite at 800 °C.³⁹ Chou and coworkers⁴⁰ have observed that hole transfer from hematite surface states depends on the deposition method. In particular, by measuring the low frequency capacitance associated with

surface states, they have shown that hole transfer from these states is more favorable for oxidation of Fe than for anodic electrodeposition. In the case of hematite obtained by vapor deposition in 1 M NaOH, a 580 nm spectral signal has been observed by Durrant's group⁴¹ using Transient Absorption Spectroscopy (TAS). They ascribed this spectral feature to a hole transition between the valence band and localized states, which were identified as iron–oxygen vacancy complexes. They also observed long lived holes at higher applied bias (>0.8 V vs. RHE) and confirmed these results by IS;¹⁸ however, these results may be influenced by parasitic faradic processes at such large bias.

Doyle and coworkers⁴² obtained similar results to those of hematite for the pH dependence of hydrous iron oxide. Through IS measurements, they observed a direct pH dependence of the low frequency capacitance. For very basic aqueous solution (concentration of NaOH superior to 1 mol L⁻¹), they observed a clear capacitive peak associated with surface states, which they identified as Fe=O intermediaries. In contrast, for lower concentrations of NaOH (inferior to 0.5 mol L⁻¹), they measured a capacitance similar to the valence band capacitance displayed in Fig. 4 (plot 1).

Finally, the presence of a hole scavenger or an over-layer for catalysis or passivation purposes strongly influences the nature of the hole transfer process. In the presence of hole scavengers such as $[\text{Fe}(\text{CN})_6]^{3-/4-}$,⁴³ H_2O_2 ,⁴⁴ or CH_3OH ,⁹ hematite does not present the capacitive peak behavior induced by surface states and direct hole transfer from the valence band is certainly occurring. In this case, the IS pattern is a single semicircle that is associated with the semiconductor capacitance ($C_{\text{out}}^{\text{cb}}$) in the ECs in Fig. 3), which allows for obtaining the Mott–Schottky plot of the material. It is however unfeasible to observe with IS the low frequency valence band capacitance (C_{v}^{vb}) for such large band gap materials. In the presence of an over layer such as Co-Pi,⁴⁹ IrO_x ⁴⁵ on hematite, it has been observed that the hole transfer resistance is decreased. In some cases, the oxide layer increases hole recombination, as in the case of MnO_x .⁴⁶ In addition, such layers generally introduce a capacitance which hides the surface state capacitance. In this case, the overlayer allows accumulation of holes and reduces surface recombination.⁴⁷ However, in this situation it is a complex task to ascribe the diminution of recombination to an increase of the charge transfer kinetics only or to a concomitant passivation of the surface states. As stated by Sivula, the term catalyzer takes a whole new dimension for semiconductors.⁴⁸ An example is the study performed by Riha and coworkers who have observed a significant improvement in the onset voltage and photo-current when depositing an ultrathin layer of $\text{Co}(\text{OH})_2/\text{Co}_3\text{O}_4$ on top of hematite by ALD.⁴⁹ Their EIS analysis revealed a decrease in the surface state capacitance and charge transfer resistance. In this case, the passivating layer allowed improving the kinetics of hole transfer as well as decreasing the density of surface states.

Conclusion

Two hole transfer processes have been discussed for the oxidation reaction at the interface semiconductor/electrolyte. The first one is a direct hole transfer from the valence band. The

second one is an indirect charge transfer from surface states. We have performed full drift-diffusion simulations and have shown that independent of the charge transfer process the hole concentration at the semiconductor/electrolyte must saturate at higher anodic bias, and so does the anodic current. In addition, we have shown that surface states may be an asset for fuel production since good charge transfer kinetics from these states can provide lower onset voltages as well as higher anodic current. In the dynamic regime, we have shown that both charge transfer processes can be modelled by the same EC when applying the IS method. However the nature and voltage behavior of the electrical elements of both ECs are different. In particular, the low frequency capacitance associated with the valence band holes for the direct charge transfer model shows saturation at higher voltage. In contrast, the one related to the surface state holes for the indirect charge transfer model displays a peak behavior with voltage. However the capacitive behavior is strongly dependent on the nature of the semiconductor/electrolyte interface.

Acknowledgements

The research leading to these results has received funding from the European Union Seventh Framework Program [FP7/2007-2013] under grant agreement 316494 and MINECO of Spain under project MAT2013-47192-C3-1-R. This work was also supported by Ministerio de Educación y Ciencia under research Grant FPU12/02712, and under research Project from MINECO, TEC2013-47283-R.

References

- 1 A. J. Nozik, *Annu. Rev. Phys. Chem.*, 1978, **29**, 189.
- 2 M. A. Butler and D. S. Ginley, *J. Mater. Sci.*, 1980, **15**, 1–19.
- 3 J. Bolts and M. Wrighton, *J. Phys. Chem.*, 1976, **80**, 2641–2645.
- 4 M. G. Walter, E. L. Warren, J. R. McKone, S. W. Boettcher, Q. Mi, E. A. Santori and N. S. Lewis, *Chem. Rev.*, 2010, **110**, 6446–6473.
- 5 A. Fujishima and K. Honda, *Nature*, 1972, **238**, 37–38.
- 6 Y. Zhang, Y. Guo, H. Duan, H. Li, C. Sun and H. Liu, *Phys. Chem. Chem. Phys.*, 2014, **16**, 24519–24526.
- 7 C. Santato, M. Ulmann and J. Augustynski, *J. Phys. Chem. B*, 2001, **105**, 936–940.
- 8 H. K. John and K. W. Frese, Jr., *J. Electrochem. Soc.*, 1978, **125**, 709–714.
- 9 B. Klahr, S. Gimenez, O. Zandi, F. Fabregat-Santiago and T. Hamann, *ACS Appl. Mater. Interfaces*, 2015, **7**, 7653–7660.
- 10 L. M. Peter, K. G. U. Wijayantha and A. A. Tahir, *Faraday Discuss.*, 2012, **155**, 309–322.
- 11 J. Tang, J. R. Durrant and D. R. Klug, *J. Am. Chem. Soc.*, 2008, **130**, 13885–13891.
- 12 B. Klahr, S. Gimenez, F. Fabregat-Santiago, T. Hamann and J. Bisquert, *J. Am. Chem. Soc.*, 2012, **134**, 4294–4302.
- 13 K. Maeda and K. Domen, *J. Phys. Chem. Lett.*, 2010, **1**, 2655–2661.
- 14 S. Y. Reece, J. A. Hamel, K. Sung, T. D. Jarvi, A. J. Esswein, J. J. H. Pijpers and D. G. Nocera, *Science*, 2011, **334**, 645–648.
- 15 Y. Tachibana, L. Vayssieres and J. R. Durrant, *Nat. Photonics*, 2012, **6**, 511–518.
- 16 L. Bertoluzzi and J. Bisquert, *J. Phys. Chem. Lett.*, 2012, **3**, 2517–2522.
- 17 P. Salvador and C. Gutierrez, *J. Phys. Chem.*, 1984, **88**, 3696–3698.
- 18 F. Le Formal, S. R. Pendlebury, M. Cornuz, S. D. Tilley, M. Grätzel and J. R. Durrant, *J. Am. Chem. Soc.*, 2014, **136**, 2564–2574.
- 19 B. Klahr, S. Gimenez, F. Fabregat-Santiago, J. Bisquert and T. W. Hamann, *J. Am. Chem. Soc.*, 2012, **134**, 16693–16700.
- 20 J. Bisquert, *Phys. Chem. Chem. Phys.*, 2003, **5**, 5360–5364.
- 21 J. Bisquert and R. Marcus, in *Multiscale Modelling of Organic and Hybrid Photovoltaics*, ed. D. Beljonne and J. Cornil, Springer, Berlin Heidelberg, 2014, vol. 352, ch. 471, pp. 325–395.
- 22 J. Reichman, *Appl. Phys. Lett.*, 1980, **36**, 574–577.
- 23 P. Cendula, S. D. Tilley, S. Gimenez, J. Bisquert, M. Schmid, M. Grätzel and J. O. Schumacher, *J. Phys. Chem. C*, 2014, **118**, 29599–29607.
- 24 I. Mora-Seró, T. Lana-Villarreal, J. Bisquert, A. Pitarch, R. Gómez and P. Salvador, *J. Phys. Chem. B*, 2005, **109**, 3371–3380.
- 25 J. Bisquert, L. Bertoluzzi, I. Mora-Sero and G. Garcia-Belmonte, *J. Phys. Chem. C*, 2014, **118**, 18983–18991.
- 26 J. Bisquert, *J. Electroanal. Chem.*, 2010, **646**, 43–51.
- 27 Z. Hens, *J. Phys. Chem. B*, 1999, **103**, 122–129.
- 28 E. A. Ponomarev and L. M. Peter, *J. Electroanal. Chem.*, 1995, **397**, 45–52.
- 29 Y. Nakato, A. Tsumura and H. Tsubomura, *J. Phys. Chem.*, 1983, **87**, 2402–2405.
- 30 K. Schwanz, U. Weiler, R. Hunger, T. Mayer and W. Jaegermann, *J. Phys. Chem. C*, 2006, **111**, 849–854.
- 31 L. Bertoluzzi, I. Herraiz-Cardona, R. Gottesman, A. Zaban and J. Bisquert, *J. Phys. Chem. Lett.*, 2014, **5**, 689–694.
- 32 D. Monroe and M. A. Kastner, *Phys. Rev. B: Condens. Matter Mater. Phys.*, 1986, **33**, 8881–8884.
- 33 F. Nunzi, E. Mosconi, L. Storchi, E. Ronca, A. Selloni, M. Grätzel and F. De Angelis, *Energy Environ. Sci.*, 2013, **6**, 1221–1229.
- 34 C. Fàbrega, D. Monllor-Satoca, S. Ampudia, A. Parra, T. Andreu and J. R. Morante, *J. Phys. Chem. C*, 2013, **117**, 20517–20524.
- 35 P. Reckers, M. Dimamay, J. Klett, S. Trost, K. Zilberberg, T. Riedl, B. A. Parkinson, J. Brötz, W. Jaegermann and T. Mayer, *J. Phys. Chem. C*, 2015, **119**, 9890–9898.
- 36 L. Bertoluzzi, L. Badia-Bou, F. Fabregat-Santiago, S. Gimenez and J. Bisquert, *J. Phys. Chem. Lett.*, 2013, **4**, 1334–1339.
- 37 B. Iandolo and A. Hellman, *Angew. Chem., Int. Ed.*, 2014, **53**, 13404–13408.
- 38 B. Klahr and T. Hamann, *J. Phys. Chem. C*, 2014, **118**, 10393–10399.
- 39 O. Zandi and T. W. Hamann, *J. Phys. Chem. Lett.*, 2014, **5**, 1522–1526.

- 40 J.-C. Chou, S.-A. Lin, C.-Y. Lee and J.-Y. Gan, *J. Mater. Chem. A*, 2013, **1**, 5908–5914.
- 41 M. Barroso, S. R. Pendlebury, A. J. Cowan and J. R. Durrant, *Chem. Sci.*, 2013, **4**, 2724–2734.
- 42 R. L. Doyle and M. E. G. Lyons, *Phys. Chem. Chem. Phys.*, 2013, **15**, 5224–5237.
- 43 B. Klahr, S. Gimenez, F. Fabregat-Santiago, J. Bisquert and T. W. Hamann, *Energy Environ. Sci.*, 2012, **5**, 7626–7636.
- 44 H. Dotan, K. Sivula, M. Gratzel, A. Rothschild and S. C. Warren, *Energy Environ. Sci.*, 2011, **4**, 958–964.
- 45 L. Badia-Bou, E. Mas-Marza, P. Rodenas, E. M. Barea, F. Fabregat-Santiago, S. Gimenez, E. Peris and J. Bisquert, *J. Phys. Chem. C*, 2013, **117**, 3826–3833.
- 46 X. Yang, C. Du, R. Liu, J. Xie and D. Wang, *J. Catal.*, 2013, **304**, 86–91.
- 47 M. Risch, F. Ringleb, M. Kohlhoff, P. Bogdanoff, P. Chernev, I. Zaharieva and H. Dau, *Energy Environ. Sci.*, 2015, **8**, 661–674.
- 48 K. Sivula, *J. Phys. Chem. Lett.*, 2013, **4**, 1624–1633.
- 49 S. C. Riha, B. M. Klahr, E. C. Tyo, S. Seifert, S. Vajda, M. J. Pellin, T. W. Hamann and A. B. F. Martinson, *ACS Nano*, 2013, **7**, 2396–2405.